ELSEVIER

Astroparticle Physics 8 (1998) 213–221

Astroparticle Physics

Stereoscopic observations of gamma rays at the Whipple observatory

F. Krennrich [a,*], C.W. Akerlof [b], J.H. Buckley [d], J. Bussóns-Gordo [f], D.A. Carter-Lewis [a], M.F. Cawley [e], M.A. Catanese [a], V. Connaughton [f], D.J. Fegan [f], J.P. Finley [g], J.A. Gaidos [g], K.H. Harris [d], A.M. Hillas [c], R.C. Lamb [a], M.J. Lang [h], G. Mohanty [a], J. Quinn [f], A.J. Rodgers [c], H.J. Rose [c], A.C. Rovero [i], M.S. Schubnell [b], G.H. Sembroski [g], T.C. Weekes [d], C. Wilson [g]

[a] *Department of Physics and Astronomy, Iowa State University, Ames, IA 50011-3160, USA*
[b] *Randall Laboratory of Physics, University of Michigan, Ann Arbor, MI 48109-1120, USA*
[c] *Department of Physics, University of Leeds, Leeds, LS2 9JT, Yorkshire, England, UK*
[d] *Fred Lawrence Whipple Observatory, Harvard-Smithsonian CfA, P.O. Box 97, Amado, AZ 85645-0097, USA*
[e] *Physics Department, St.Patrick's College, Maynooth, County Kildare, Ireland*
[f] *Physics Department, University College, Dublin 4, Ireland*
[g] *Department of Physics, Purdue University, West Lafayette, IN 47907, USA*
[h] *Department of Physics, University College, Galway, Ireland*
[i] *Instituto de Astronomia y Fisica del Espacio, Buenos Aires, Argentina*

Received 25 August 1997

Abstract

Observations of photons at $E \geq 550$ GeV from the Crab Nebula are presented and used to assess the potential of multi-telescope systems for γ-ray astronomy.

The Whipple observatory 10 m and 8 m imaging atmospheric Čerenkov telescopes have been used to provide a stereoscopic view of air showers to make a more complete measurement of air shower parameters. Here we present a measurement of the spread in the arrival direction of primary γ-rays originating from a point source. The data show that the shower arrival direction can be reconstructed with an accuracy of $\sigma = 0.^{\circ}14$. © 1998 Elsevier Science B.V.

Keywords: Gamma Rays: General; Instruments; Observations: Crab Nebula

1. Introduction

The ground-based imaging atmospheric Čerenkov technique has been successfully used to detect TeV-photons ($E \geq 300$ GeV) from five galactic objects: the Crab Nebula [42], Vela pulsar [45], PSR1706-44 [19], the supernova remnant SN1006 [20], and the binary pulsar PSR1259-63 [38], and the two extragalactic sources Mrk 421 [32,33] and Mrk 501 [35,6]. At MeV–GeV energies, results from the Energetic Gamma-Ray Experiment Telescope (EGRET) on the Compton Gamma-Ray Observatory (CGRO) have established the field of MeV–GeV γ-ray astronomy through the detection of more than

* Corresponding author.

PII S0927-6505(97)00058-3

129 sources [40]. However, the EGRET observations which cutoff at 30 GeV do not yet provide answers to many basic questions regarding the origin of the observed radiation.

The energy region above 50 GeV remains the domain of ground-based Čerenkov telescopes, because they have huge collection areas (10^4–10^5 m^2) in comparison to satellite experiments [30]. The ground-based imaging atmospheric Čerenkov technique employs large optical light collectors focusing the Čerenkov light emitted by secondary particles of an air shower onto an array of fast photomultipliers covering a 3–5° field of view. The two-dimensional image of the Čerenkov light distribution in the focal plane is used to separate γ-ray induced showers from a background of cosmic-ray induced showers. Čerenkov images generated by γ-rays are characterized by narrower widths and lengths compared to cosmic-ray images, and for a point source at the center of the field of view, they are aligned parallel to the telescope optic axis, resulting in small angles between the image major axis and the line joining the image centroid and the center of the field of view (the *alpha* parameter) [36].

Although substantial improvements in sensitivity have been made by second generation Čerenkov detectors such as the Whipple Observatory 10 m telescope [7] and HEGRA [31] and CAT [4], new efforts are underway to improve the technique further. Different approaches are currently being investigated. High resolution focal plane detectors are employed in the CAT telescope [34] and will be used in the so-called GRANITE III project of the Whipple Collaboration [23]. A different approach is to better characterize γ-ray showers with a system of two or more telescopes [13,1,16] which provide multiple viewpoints of the same shower. The observation of air showers by two or more imaging atmospheric Čerenkov telescopes provides additional information that cannot be achieved with a single telescope. The stereoscopic view permits the three-dimensional reconstruction of the Čerenkov light distribution of air showers and could improve the imaging atmospheric Čerenkov technique in a number of different ways:

(a) sensitivity;
(b) γ/hadron separation;
(c) angular resolution;
(d) energy resolution;
(e) energy threshold.

The sensitivity is partially improved by the bigger collection area of multiple telescopes as well as a better background suppression for the coincident events. Points (b),(c) are directly linked to improve the sensitivity of multi-telescope systems. The accuracy of measuring air shower parameters such as the arrival direction and the energy of the primary photon will improve the quality of those measurements. This may lead to a sharper classification of the type of air shower (γ-ray or hadronic), to distinguish a γ-ray primary from a cosmic-ray primary. In addition, the stereoscopic view provides information of the shower core impact point on the ground which is currently missing in measurements with a single telescope. The information about the shower core is crucial to improve the energy resolution of the imaging atmospheric Čerenkov technique. Stereo detectors may also play an important role in lowering the energy threshold [22,16] of atmospheric Čerenkov detectors. Large scale imaging atmospheric Čerenkov detectors such as VERITAS [44] and HESS [2], employing 9–16 telescopes operating at an energy threshold of $E \geq 50$ GeV, have been proposed as a major step to improve the sensitivity of ground-based γ-ray observatories. Some experimental data from multi-telescope installations are present in the literature [9,21,2].

The Whipple collaboration has pursued the stereo approach with the 10 m–8 m stereo system to test some aspects of the performance in the few hundred GeV region and results are presented here. The 10 m telescope is routinely operated in an extensive observing program of γ-ray sources. The 8 m telescope (originally 11 m) was built as a low-cost test-experiment and was used as an auxiliary telescope together with the 10 m telescope. The investigations were limited because the 8 m auxiliary telescope suffered from mechanical rigidity problems, had low UV reflectivity and was located at the rather large distance of 146 meters from the 10 m reflector (dictated by local geography). Nevertheless, we were able to detect a coincident signal from the Crab Nebula and have explored some aspects of the stereoscopic technique in the few hundred GeV region. We were able to make a direct measurement of the errors associated with inferring the arrival directions of primary gamma rays.

In this paper we examine the simplest aspects of the stereo technique using experimental data recorded

with the Whipple Observatory 10 m and 8 m telescopes, more detailed studies will be discussed elsewhere. In Section 2 we describe the 10 m and 8 m telescope system. In Section 3 the stereo observations of the Crab Nebula are presented. The method of stereoscopic analysis is described in Section 4. The results of the observations are presented in Section 5. In Section 6 we summarize and discuss the implications of these measurements.

2. The stereo detector

Measurements reported here were carried out with two telescopes: the well-proven 10 m Whipple Observatory γ-ray detector [7] and an auxiliary 8 m telescope (see Table 1). The stereo detector has been constructed on the southern ridge of Mount Hopkins near Amado, Arizona at a latitude of 31° 41' and an altitude of 2300 meters. Limited space on the ridge determined the location of the second telescope (8 m) relative to the existing Whipple Observatory 10 m telescope and resulted in the spacing of 146 m between the two instruments. The 8 m telescope was first put into operation in December 1995 with a 91 pixel camera for stereoscopic observations in conjunction with the 10 m telescope.

The second telescope consists of a tessellated parabolic reflector with an effective diameter of 8 m. The mount and optical support structure (OSS) came from a solar reflector built by McDonnell-Douglas for solar energy research. The mechanical structure of the OSS is less rigid than the existing 10 m telescope and therefore the expected performance is below its 10 m companion.

The optical reflector consists of 390 individual mirrors mounted on a parabolic surface. The total reflective mirror surface is $\approx$ 55 m^2. Budget considerations as well as the mechanical strength of the OSS of the solar reflector precluded solid ground-glass mirrors and dictated an alternative mirror design. These consist of second-surface 0.7 mm thick glass mirrors bonded to foam glass blocks which had been machined to the required radius of curvature [41]. Their primary reflectivity is in the 330–470 nm wavelength range. While the reflectivity of the 10 m telescope extends well into the UV-range (240 nm), the 8 m reflectivity drops substantially below 330 nm. This causes the 8 m reflector to collect less light from an air shower per square meter of mirror area than the 10 m reflector. Because the OSS flexes with elevation, it was necessary to align the mirrors with the reflector directed close to the zenith. A reasonable optical resolution of the combined mirrors was achieved using a vertical mirror alignment scheme with 2 lasers to adjust each individual mirror of the 8 m telescope. The two-dimensional point spread function achieved with this method has a FWHM of 0.°22 for zenith angles 0–35°.

Table 1
The stereo detector

Telescope	10 m	8 m
reflector Ø	10 m	8 m
reflector shape	Davies–Cotton	parabola
focal length	7.3 m	7.6 m
mirror area	75 m^2	55 m^2
PSF	0.°12	0.°22
# of pixels	109	91
light-cones	yes	yes
tracking accuracy	0.°03	0.°05
energy threshold	250 GeV	500 GeV

The focal plane detector consists of a two-dimensional hexagonal array of 91 1-1/8" photomultipliers (Hamamatsu R1398). The camera also includes light-cones to improve the light collection efficiency in the focal plane. The pixel spacing is 0.°25 and covers a 2.°75 wide field of view. The signals are transmitted through RG-8 coax-cable for the inner 37 phototubes (originally designed for a 37 pixel camera) and RG-58 for the outer channels to an electronics hut 50 feet from the telescope. The signals have a FWHM of less than 9 ns when they reach the data acquisition electronics. The signals feed into custom-built amplifier-discriminator modules [25]. The discriminator outputs go into a coincidence logic consisting of 32-channel majority logic units (LeCroy 4532) and a trigger logic controlled by the data acquisition computer (Vax Station 4000/90). The trigger logic requires two channels out of 91 pixels to exceed a discriminator threshold of 55 mV within a coincidence gate of 30 ns.

The interface to the data acquisition is based on the CAMAC system and is very similar to the 10 m telescope system [37]. The data acquisition is designed to operate both independently and in coincidence with the 10 m telescope. For the data reported

here, both telescopes have been operated independently. The tracking of the 8 m telescope is performed by a PC-controlled tracking system which consists of 3-phase AC-motors and motor controller. The motor controller was upgraded in summer 1996, to allow ramping for smooth acceleration and deceleration. The actual position of the telescope axes is given by 15-bit gray-coded absolute-encoders with an accuracy of 0.°01.

For the observations presented here, the 10 m telescope was equipped with a 109 pixel camera and is described in detail elsewhere [7]. It is important to emphasize that the performance of the stereo technique depends on the particular configuration of the telescopes. The telescopes used are not identical and the following points are relevant for the performance of the stereoscopic system.

(1) The FWHM of the point spread function of the 8 m telescope reflector is broader by a factor of 2 than for the 10 m telescope. This property impacts on the image quality and diminishes somewhat the distinction between hadronic and γ-ray initiated showers. However, the point spread function of the 8 m telescope (FWHM = 0.°22) still matches the pixel spacing in the focal plane (0.°25) and therefore only a marginal degradation of the imaging technique is expected.

(2) The spectral range of the light reflected by the 8 m telescope is much less than that reflected by the other telescope: while the 10 m reflectivity extends well into the UV-range (240 nm), the 8 m reflectivity begins to drop substantially below 330 nm [41]. As a result, the energy threshold (defined as the energy where the detection of gamma-rays has its maximum) of the 8 m telescope is higher than for the 10 m telescope. The energy threshold of the 8 m telescope is quoted here relative to the 10 m energy threshold and the details of the calibration are given in Section 4.3. Furthermore, the lack of UV-light reduces the r.m.s. width of hadronic showers due to a smaller contribution from local particles and therefore reduces the capability of distinguishing hadron showers from γ-ray induced showers.

(3) The tracking accuracy, provided by an analytical correction for mechanical deflections, is such that a source stays within 0.°05 of the telescope optical axis. This is similar to the tracking accuracy of the 10 m telescope (0.°03) and the effect on the angular resolution of the stereo system is negligible.

(4) The 8 m telescope is limited by the mechanical strength of the solar collector design and could not be operated if wind speeds were more than 15 miles per hour. Furthermore, due to the low thermal conductivity of the mirrors, condensation is a severe problem during the winter months excluding this instrument from regularly scheduled observations.

The sensitivity of the stereo system is limited by the sensitivity of the weakest member, in this case the 8 m telescope. However, the 8 m has a relatively low energy threshold 550 GeV (see Section 5.2), a reasonable optical resolution and a good tracking accuracy and thus it is well suited to explore some aspects of the stereoscopic imaging technique.

3. Observations

The stereo system was tested using observations of the Crab Nebula. Since γ-ray emission from the Crab Nebula is steady [43], it has become the standard candle for ground-based γ-ray astronomy, and it is the ideal source to test the performance of the stereo system. A total of 5.45 hours ON-source observations and the same amount of OFF-source measurements under clear-sky conditions were recorded during October and November 1996. Since we are exploring a new technique, the most conservative method of measuring the background was used: for each ON-source run lasting 28 minutes a corresponding OFF-source run was recorded at the same elevation and azimuth region. For each telescope the contemporaneous data were recorded individually and 10 m + 8 m events identified with an absolute time accuracy of 250 μs, provided by two GPS clocks.

4. Stereo analysis

4.1. Event selection

Stereo coincidences are found in the off-line analysis by matching the time of the events in both telescopes. Events from the data of the two telescopes are

Table 2
Cuts used in stereo analysis

Parameter	10 m	8 m
width:	$0.^\circ07 \leq$ width $\leq 0.^\circ17$	-
length:	$0.^\circ16 \leq$ length $\leq 0.^\circ34$	-
distance:	$0.^\circ51 \leq$ distance $\leq 1.^\circ1$	$0.^\circ30 \leq$ distance $\leq 0.^\circ85$
size:	size $\geq$ 200 d.c.	size $\geq$ 100 d.c.

accepted as coincidences if their recorded times differ by less than 500 μs. This time window has been chosen to be efficient in suppressing random coincidences to a fraction of $\leq$10% at the trigger level and to allow for 100% efficiency of air shower coincidences. A *size* cut (*size* = total amount of light of the image measured in digital counts by the Analog-to-Digital-Converters) for both telescopes reduces random coincidences caused by night-sky noise significantly. The *size* selection also ensures a minimum image quality to provide a robust image parametrization.

Table 2 shows the selection criteria used for the subsequent analysis. The image analysis of the stereo events has been developed with emphasis on the superior imaging quality of the 10 m telescope: shape cuts such as *width* and *length* have been applied only to the 10 m telescope images to select candidate γ-ray events. A *distance* cut for the 10 m and 8 m images has been used in order to reject images that are truncated at the edge of the field of view. The 8 m telescope camera with 91 photomultipliers requires a smaller *distance* cut than for the 10 m telescope equipped with 109 photoelements. The cuts shown in Table 2 are applied in the following analysis. These cuts differ from the standard 'Supercuts' to allow for a bigger collection area.

4.2. Reconstruction of the arrival direction

For a single telescope, the orientation parameter *alpha* [36] provides one projection of the arrival direction. A single telescope does not allow the unambiguous reconstruction of the arrival direction, however, methods have been developed [3,24,10] to derive the point of origin for a sample of events.

The stereoscopic view of the Čerenkov light distribution of air showers from two telescopes allows

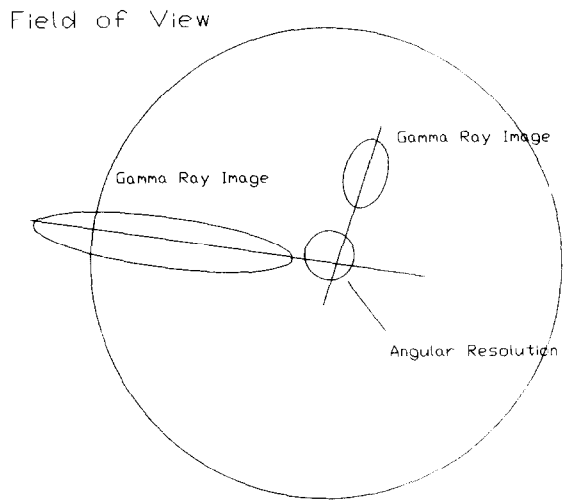

Fig. 1. Showing the principle of the arrival direction reconstruction using the two images of a stereoscopic event recorded by two telescopes. The two images characterized by their elliptical shape as they occur in a common coordinate system with respect to the sky provide information about the arrival direction of the air shower. The intersection of their major image axes points towards the arrival direction. If the origin of the coordinate system is pointed towards a γ-ray point source, the intersection points are expected to cluster in the center of the coordinate system.

the unique derivation of the arrival direction (Fig. 1) from the intersection of the major axes of the two superimposed images. This intersection point corresponds to the arrival direction of the shower on the sky with an accuracy that can be quantified by the angular resolution. This reconstruction only fails for showers falling close to the connecting line between the two telescopes.

The parameter Θ describes the angular distance of a reconstructed shower direction from the source position. A cut on Θ reduces the isotropic background from cosmic-ray induced showers. The search for point sources with the maximum sensitivity is deter-

mined by the angular resolution of the instrument. We define the angular resolution σ_{72} from a two-dimensional Gaussian function as shown in Eq. (1),

$$g(\Theta) = \frac{1}{2\pi\sigma^2} e^{-(\Theta^2)/2\sigma^2}. \quad (1)$$

We define the angular resolution as

$$\sigma_{72} = \sqrt{2}\,\sigma \quad (2)$$

and corresponds to the radius of an aperture containing 72% of all events. This search window gives optimum sensitivity for point sources.

For the arrival direction reconstruction of showers of the data we chose as a reference system a grid covering a space angle of 3° × 3° on the sky. This corresponds roughly to the field of view of the 10 m telescope. The grid system is divided into 30×30 bins with a cell size of 0.°1. We form a two-dimensional histogram by testing for each cell on the grid if a shower passes the shape cuts and a Θ-cut consistent with the source originating in the center of the individual cell. By carrying out this process for every shower in the data sample a two-dimensional histogram is formed (similar to [3]). The Θ-cut has been determined from simulations as described in Section 4.3.

It should be pointed out that the angular resolution defined here is a measure of the error associated with the reconstruction of individual γ-ray primaries. The accuracy for point source location increases with statistics and can be substantially better than the angular resolution.

In Section 5.1 we examine observations of the Crab Nebula regarding the arrival direction of the excess events using the analysis described.

4.3. Monte Carlo simulation of the stereo detector

We have simulated the response of the 10 m/8 m telescope configuration using Monte Carlo programs developed at Iowa State University [29], which are based on the KASKADE shower simulation code written by Kertzman & Sembroski [18]. The 10 m and 8 m detectors are simulated including their individual mirror reflectivity as a function of the wavelength and their different optical design – the Davies–Cotton design of the 10 m [11] and the parabolic reflector design of the 8 m telescope. The simulation [26] reproduces the measured point spread functions of FWHM

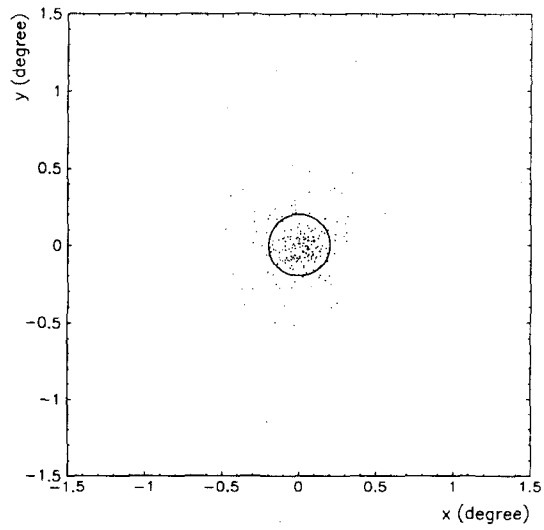

Fig. 2. Showing the arrival direction for simulated γ-rays coming from a point source aligned with the origin of the focal plane coordinate system. The intersection method has been used to reconstruct the arrival direction as described in Section 4.2. More than 72% of all the events fall within a circle of 0.°20.

= 0.°12 for the 10 m and FWHM = 0.°22 for the 8 m, respectively. The simulations have been used to derive two basic parameters of the stereo detector: (a) the angular resolution for the detection of a point source and (b) the energy threshold of the telescopes for coincident γ-ray induced air shower events.

Angular resolution To calculate the angular resolution, we have reconstructed the arrival direction of simulated coincident γ-ray events using the intersection of the major image axes. The image selection criteria as described in Section 4.1 have been used. Fig. 2 shows the pointing direction of images from γ-ray induced air showers originating from a point source which is aligned with the center of the focal plane coordinate system. As can be seen from Fig. 2, most reconstructed events (72%) fall within a radius of 0.°20 from the source. Fitting a two-dimensional Gaussian function to the event distribution in Fig. 2 shows that the accuracy of reconstructing the arrival direction is σ = 0.°14.

Energy threshold The energy threshold of the 8 m telescope and the stereo system can be calibrated by using the relative *size* ratio size(8 m)/size(10 m)

of 10 m images and 8 m images. Considerable effort has gone into the energy calibration of the 10 m telescope [5,29,17]. Here we assume that the energy threshold of the 10 m telescope has been estimated correctly and relate the threshold of the 8 m telescope directly to this value. The biggest uncertainty in the derivation of the energy threshold of the detector itself arises from the knowledge of the conversion of photoelectrons into digital counts (pe/dc-factor hereafter). The unit digital counts is used to measure the light of each pixel or the total light of an image with Analog-to-Digital-Converters (ADCs). The pe/dc-factor for the 10 m telescope has been carefully determined using different methods [29,17] and is consistent with 1 pe/dc = 1.05 ± 0.1. This factor is used to convert the number of photoelectrons produced by a simulated γ-ray shower into the number of digital counts contained in a real air shower image. The pe/dc-factor of the 8 m telescope can be derived by a cross-calibration with the 10 m telescope using coincident γ-ray shower images. Since we use the same phototubes operated at the same average voltage, the same amplification factor and ADCs (LeCroy 2249A) as in the 10 m telescope, we expect the pe/dc-factor for the 8 m telescope to be also close to 1, however in the following we derive this number from a cross-calibration based on the known 10 m energy threshold.

The *size* of an air shower image can be used as a means of estimating the energy of the primary γ-ray. In measurements with a single telescope, the *energy/size* correlation is diminished by averaging over a range of shower core distances. With two telescopes the shower core distance can be reconstructed and therefore the *energy/size* correlation is better defined. Here we make use of the *energy/size* correlation to cross-calibrate between the two telescopes to determine the pe/dc-factor of the 8 m relative to the 10 m telescope. We reconstruct the shower core position and then use only events that have a shower core distance of 60–120 m from each telescope, a region where the lateral Čerenkov light distribution for γ-ray induced air showers is relatively flat. We compare the size ratio size 8 m[dc]/size 10 m[dc] of γ-ray images from the data with size ratio size 8 m[pe]/size 10 m[pe] of simulations in units of photoelectrons. Since we know the pe/dc-factor for the 10 m telescope, the pe/dc-factor for the 8 m telescope can be derived. In Section 5.2 the results of the calibration using a γ-ray signal from the Crab Nebula are shown.

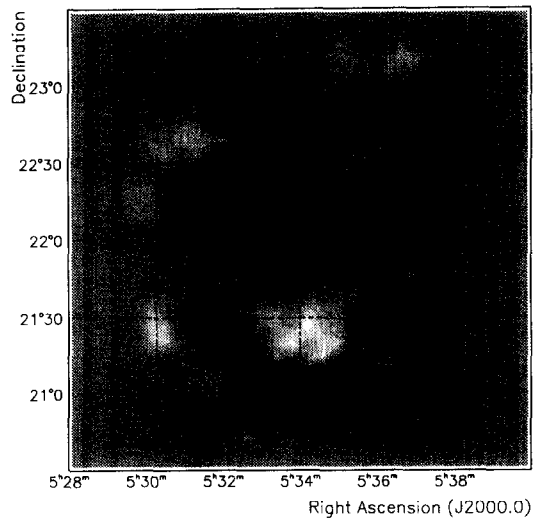

Fig. 3. The two-dimensional reconstruction of the arrival direction of air showers is shown for 5.45 hours of ON-source observations minus the OFF-source observations of the Crab Nebula. It can be seen that a clear signal is present in the data. The gray scale indicates the number of excess events (ON-source minus OFF-source) passing the cuts of Table 2. Both telescopes have been pointing at source position during the ON-source runs corresponding to the center of the camera. The excess in the contour plot coincides with the source direction of the Crab Nebula as indicated by the cross.

Table 3
Results for coincident events for the Crab Nebula observations

Energy	Excess	Significance
0.550 TeV	85±11	7.9σ

5. Results from the Crab Nebula observations

5.1. Angular resolution

Fig. 3 shows the results of the two-dimensional analysis (as described in Section 4.2) of the arrival direction for coincident, candidate γ-ray events from stereo observations of the Crab Nebula. The gray scale in the histogram indicates the number of excess events (ON-source minus OFF-source) passing the cuts of Table 2 and $\Theta \leq 0.^{\circ}20$. The contours show the likelihood ratio test statistic in 1σ steps based on the method of Li and Ma [27] as derived from the number of counts ON-source and OFF-source. For this analysis (see Ta-

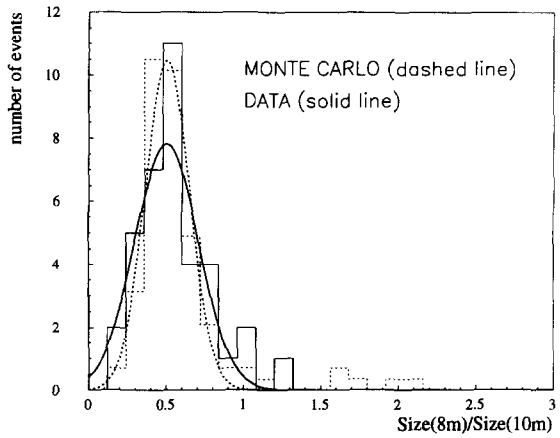

Fig. 4. The *size* ratio (size(8 m)/size(10 m)) is being used to test the relative calibration of the photoelectron to digital count the conversion factor for the 8 m telescope. Since both distribution of the size ratio, the simulated events and the data are centered at the same value, the pe/dc-factor of the 8 m telescope is close to 1 (0.96 ± 0.1). It can also be seen that the average *size* of the 8 m images is by a factor of 2 smaller than for the 10 m telescope.

ble 3) the significance is 7.9σ (85 ± 11 excess events). The excess is consistent with the source position as indicated by the cross in Fig. 3. The angular resolution $\sigma_{72} = 0.°20$ ($\sigma = 0.°14$) for the two-dimensional analysis at the given *size* threshold (size 10 m $\geq$ 200 d.c., size 8 m $\geq$ 100 d.c.) has been derived from the data and is consistent with the prediction from the simulation results showing the maximum significance for a search window of 0.°20.

5.2. Cross-calibration of the energy threshold

In Section 4.3 we have described the method to derive the energy threshold of the 8 m telescope from a cross-calibration with the 10 m telescope, for which the energy threshold is known. The shower core has been reconstructed for the coincident events using the cuts as mentioned above. Only events with a reconstructed shower core distance of 60–120 m from each telescope have been accepted to compare the size ratio size 8 m[dc]/size 10 m[dc].

Fig. 4 shows the size ratio for the ON-source data (in units of dc) and for the simulations (in units of pe). The center position of the two distributions agree within 5% and we conclude that the pe/dc-factor conversion factor of the 8 m telescope is consistent with 0.96 ± 0.1. Fig. 4 also shows that the 8 m telescope detects about two times less light than the 10 m telescope. Therefore, the energy threshold of the 8 m telescope is consistent with 500 GeV at a given trigger condition similar to the 10 m trigger. The energy threshold for coincident events is consistent with 550 GeV for events passing a threshold of size 8 m $\geq$ 100 d.c. and size 10 m $\geq$ 200 d.c., whereas the energy threshold for the 10 m alone is 250 GeV at the trigger level.

6. Discussion and summary

The Whipple observatory stereo detector has been used to test some aspects of the stereoscopic imaging atmospheric Čerenkov technique in the 500 GeV region. It has been demonstrated by using Crab Nebula observations that the stereoscopic approach of reconstructing the arrival direction of γ-rays from a point source can be used to improve the resolution of imaging atmospheric Čerenkov telescopes. With a system of two telescopes with a pixel spacing of 0.°25 an angular resolution of σ_{72}=0.°20 (σ=0.°14) can be reached. Extrapolating this result for arrays like VERITAS where 9 telescopes with pixel sizes of 0.°12 and 0.°23 are proposed, an accuracy of σ_{72}= 0.°03–0.°06 seems achievable. This is based on the extrapolation with the square root of the number of telescopes presuming that 9 telescopes contribute to the stereoscopic view. A limit to this extrapolation occurs due to the shower development itself and Hillas [14] has shown that the limit is in the range of 0.°025 for 500 GeV γ-ray primaries. By standards of other γ-ray detectors on the CGRO ($E \leq 20$ GeV), the ground-based imaging atmospheric Čerenkov technique offers a superior angular resolution to resolve γ-ray sources.

Acknowledgements

We acknowledge the technical assistance of T. Lappin. This research is supported by grants from the U.S. Department of Energy and by NASA, by PPARC in the UK and by Forbairt in Ireland.

References

[1] F.A. Aharonian et al., in: Towards a Major Atmospheric Čerenkov Detector, Calgary, R.C. Lamb, ed. (1993) p. 81.

[2] F.A. Aharonian et al., Proc. of 4th Compton Symp. (1997), to be published.
[3] Akerlof et al., Ap. J. 377 (1991) L97.
[4] A. Barrau et al., Proc. of 25th Int. Cosmic Ray Conf., Durban, Vol. 3 (1997) p. 173.
[5] S.D. Biller et al., Proc. of 24th Int. Cosmic Ray Conf., Rome, Vol. 3 (1995) p. 412.
[6] S. Bradbury et al., A & A (1997), in press.
[7] M.F. Cawley et al., Exp. Astr. 1 (1990) 173.
[8] M.F. Cawley, T.C. Weekes, Exp. Astr. 6 (1995) 7.
[9] P.M. Chadwick et al., Workshop on TeV Gamma-Ray Astrophysics, Heidelberg (1996) p. 153.
[10] V. Connaughton et al., Ap. J. 479 (1997) 859.
[11] J.M. Davies, E.S. Cotton J. Solar Energy Sci. Eng. 1 (1957) 16.
[12] J.A. Gaidos et al., Nature 383 (1996) 319.
[13] J.E. Grindlay et al., Ap. J. 201 (1975) 82.
[14] A.M. Hillas, Proc. Int. Workshop on Very High Energy Gamma Ray Astronomy, Crimea (1989) p. 134.
[15] A.M. Hillas, Proc. 19th Int. Cosmic Ray Conf., La Jolla, Vol. 3 (1985) p. 445.
[16] A.M. Hillas, Space Science Reviews, Vol. 75, Nos. 1-2 (1996).
[17] A.M. Hillas et al., Ap. J. (1997), submitted.
[18] M. Kertzman, G.H. Sembroski, NIM A 343 (1994) 629.
[19] T. Kifune et al., Ap. J. 438 (1995) L91.
[20] T. Kifune et al., in: Towards a Major Atmospheric Čerenkov Detector V, Kruger National Park (1997), in preparation.
[21] A. Kohnle et al., Astropart. Phys. 5 (1995) 119.
[22] F. Krennrich, R.C. Lamb, Exp. Astr. 6 (1995) 285.
[23] R.C. Lamb et al., in: Towards a Major Atmospheric Čerenkov Detector IV, Padua, M. Cresti, ed. (1995) 386.
[24] R.W. Lessard et al., in: Towards a Major Atmospheric Čerenkov Detector V, Kruger National Park (1997), in preparation.
[25] H. Levy, D. Frishman, C. Akerlof, NIM A 292 (1990) 715.
[26] D.A. Lewis, Exp. Astr. 1 (1990) 213.
[27] T. Li, Y. Ma, Ap. J. 272 (1983) 317.
[28] E. Lorenz et al., Proc. of the 4th Compton Symp. (1997), in press.
[29] G. Mohanty et al., Astropart. Phys. (1997), submitted.
[30] R.A. Ong, Proc. 1994 Snowmass Summer Study "Particle and Nuclear Astrophysics and Cosmology in the next Millennium" (1995) p. 110.
[31] M. Panter, Proc. of 24th Int. Cosmic Ray Conf., Rome, Vol. 1 (1995) p. 958.
[32] D. Petry et al., A & A 311 (1996) 13.
[33] M. Punch et al., Nature 358 (1992) 477.
[34] M. Punch et al., in: Towards a Major Atmospheric Čerenkov Detector, Padua, M. Cresti, ed. (1995) p. 356.
[35] J. Quinn et al., Ap. J. 456 (1996) L83.
[36] P.T. Reynolds et al., Ap. J. 404 (1993) 206.
[37] H.J. Rose et al., Proc. of 24th Int. Cosmic Ray Conf., Rome, Vol. 3 (1995) p. 766.
[38] T. Sako et al., Proc. of 25th Int. Cosmic Ray Conf., Durban, Vol. 3 (1997) p. 193.
[39] T. Tanimori et al., Ap. J. 429 (1994) L61.
[40] D. Thompson et al., Ap. J. Suppl. 101 (1995) 259.
[41] C. Weaverdyck, D. Meyer, C. Akerlof, NIM A 310 (1991) 690.
[42] T.C. Weekes et al., Ap. J. 342 (1989) 379.
[43] T.C. Weekes, Proc. 2nd Compton Symp., AIP Conf. Proc. 304, C.E. Fichtel, N. Gehrels, J.P. Norris, eds. (1994) p. 270.
[44] T.C. Weekes, Proc. of 4th Compton Symp. (1997), in press.
[45] T. Yoshikoshi et al., Institute for Cosmic Ray Research University of Tokyo, ICRR-Report-365-96-16 (1996).